Parametric Whirl Flutter Analysis of Twin Turboprop Aircraft Configuration

*Jiri Cecrdle**
**Aeronautical Research and Test Institute (VZLU)*
Beranovych 130, Prague - Letnany, 199 05, Czech Republic

Abstract
This paper addresses the whirl flutter of turboprop aircraft structures. This research examines the evaluation of the influence of the main parameters on the stability margins with respect to whirl flutter of a twin turboprop aircraft configuration. In addition, the applicability of the half-span model instead of the full-span model is presented and clarified. The evaluated parameters include the relationship of both propellers' revolutions, i.e., identical (CW/CW) or inverse (CW/CCW). Furthermore, non-symmetrical configurations, that are required to be analysed by regulation standards, such as a single propeller feathering or a single propeller overspeed were analysed. Parametric studies were performed using a reference model with four degrees-of-freedom, which represented a typical structure of a twin wing-mounted engine turboprop aircraft with flexibly attached engines in both pitch and yaw. The other structural parts were considered to be rigid.

1. Introduction

Turboprop aircraft structures are certified with respect to whirl flutter. Whirl flutter, which was discovered by Taylor and Browne [1], is a specific case of flutter, that accounts for the additional dynamic and aerodynamic effects of the engine's rotating parts. The rotating parts, such as a propeller or a gas turbine engine rotor, increase the number of degrees-of-freedom and cause additional forces and moments. Moreover, a rotating propeller causes a complicated flow field and interference effects among the wing, nacelle and propeller. Whirl flutter instability is driven by motion-induced unsteady aerodynamic propeller forces and moments that act in the propeller plane. These factors could cause the unstable vibration of a propeller mounting, which could lead to the failure of an engine installation or an entire wing.

Considering the conventional propellers of smaller turboprop commuter or utility aircraft, for which the propeller blade frequencies are much higher compared to the nacelle pitch and yaw frequencies, a simple analytical model with a rigid propeller is applied. Propeller aerodynamic forces are usually determined using Strip Theory according to the solutions of Ribner [2], [3] or Houbolt and Reed [4].

Apart from the nominal state, the influence of various parameters on the whirl flutter is required to be analysed by regulation standards. The FAR/CS 23 regulation standard for normal, utility, aerobatic and small commuter aircraft [5], [6], [7] requires analysis of the changes in the stiffness and damping of the engine mounting system (23.629(e)(2)). Moreover, the FAR/CS 25 regulation standard for larger aeroplanes [8], [9] includes requirements to analyse specific failure states (failures of the engine mount load bearing elements (25.629(d)(4)(5)), propeller feathering (25.629(d)(6)), propeller overspeed (25.629(d)(7)), and others). Moreover, for a twin tractor turboprop aircraft, the relationship of the revolutions of the two propellers, i.e., identical or inverse, is also an important factor that could influence the flutter behaviour.

2. Theoretical Background

The fundamental solution [10] is derived for the system with two degrees-of-freedom. The engine system's flexible mounting can be substituted by a system that is composed of two rotational springs (stiffness K_Ψ, K_Θ) as illustrated in figure 1. Neglecting the propeller rotation and the aerodynamic forces, the two independent mode shapes (yaw – around vertical axis, pitch – around lateral axis) will emerge as shown in figure 2 with angular frequencies of ω_Ψ and ω_Θ.

Considering the propeller rotation, the system motion changes to the characteristic gyroscopic motion. The gyroscopic effect makes two independent mode shapes merge into a whirl motion, as shown in figure 3. The propeller axis shows an elliptical movement. The orientation of the propeller axis movement is backward relative to the propeller rotation for the mode that has a lower frequency (backward whirl mode – figure 3a) and forward relative to the propeller rotation for the mode that has a higher frequency (forward whirl mode – figure 3b). This orientation corresponds to the low-speed and high-speed precession of the gyroscopic system. The mode shapes of the mentioned gyroscopic modes are complex because independent yaw and pitch modes have a phase shift of 90°. The condition of the real mode shapes corresponds to the state of a non-rotating system.

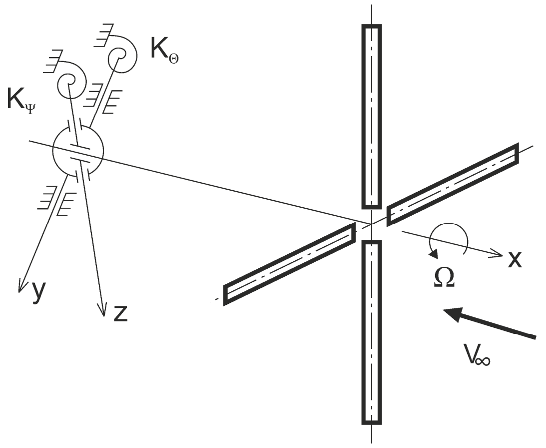

Figure 1: Gyroscopic system with propeller

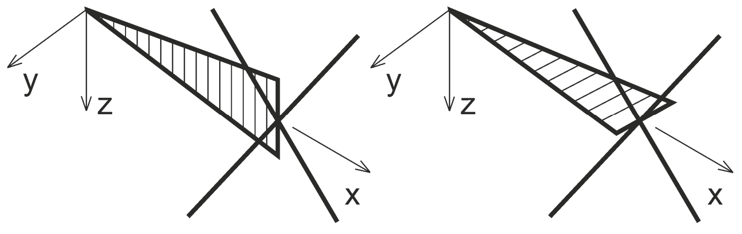

a) b)

Figure 2: Independent pitch (a) and yaw (b) mode shapes

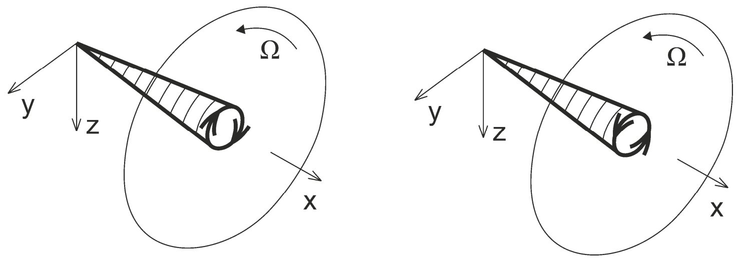

Figure 3: Backward and forward whirl mode

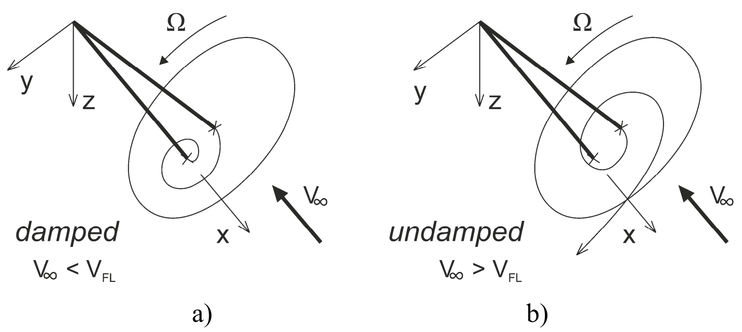

a) b)

Figure 4: Stable (a) and unstable (b) state of the gyroscopic vibrations for the backward flutter mode

The described gyroscopic mode shapes result in harmonic changes of propeller blades' angles of attack. They give rise to non-stationary aerodynamic forces, which could, under the specific conditions, induce flutter instability.

Possible states of the gyroscopic system from the flutter stability point of view for the backward mode are explained in figure 4. Provided that the air velocity is lower than a critical value ($V_\infty < V_{FL}$), the system is stable and the motion is damped. If the airspeed exceeds the critical value ($V_\infty > V_{FL}$), then the system becomes unstable and the motion is divergent. The limit state ($V_\infty = V_{FL}$) with no total damping is called the critical flutter state, and V_{FL} is called the critical flutter speed. The special case is a gyroscopic divergence, in which the frequency becomes zero and the motion changes to having a one-directional character.

The basic problem of an analytical solution is grounded on the determination of the aerodynamic forces that are caused by the gyroscopic motion of the specific propeller blades. Considering that there is no sideslip angle, the basic characteristics of the aerodynamic forces can be obtained using quasi-steady theory. The equations of motion are set up for the system described in figure 1 by means of Lagrange's approach. The kinematical scheme including the gyroscopic effects, is shown in figure 5.

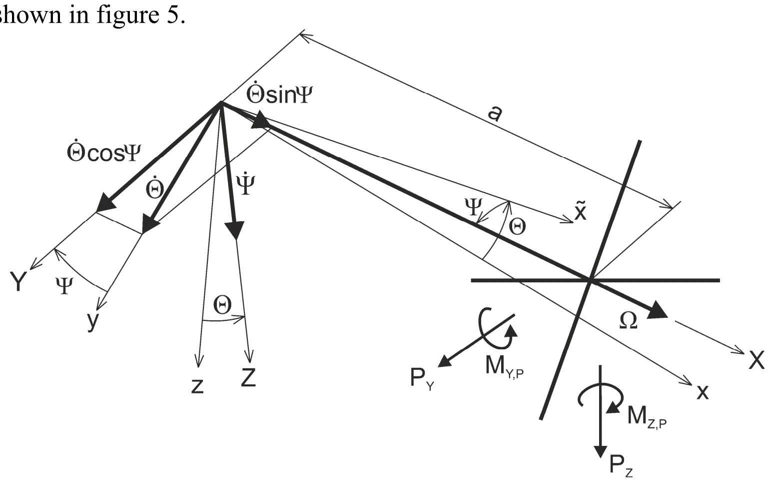

Figure 5: Kinematical scheme of the gyroscopic system

The independent generalized coordinates are three angles (φ, Θ, Ψ). The ranges for the angle Θ are <z; Z> and <x; X>, and for the angle Ψ, they are <$\tilde{x}$; X> and <y; Y>. We assume that the propeller angular velocity is constant ($\varphi = \Omega$ t), the mass distribution is symmetric around the X-axis and the mass moments of inertia are $J_Z \neq J_Y$. We will use a coordinate system X, Y, Z, which is linked to the system. Then, the kinetic energy is

$$E_K = \frac{1}{2} J_X \omega_X^2 + \frac{1}{2}\left(J_Y \omega_Y^2 + J_Z \omega_Z^2\right) \tag{1}$$

The angular velocities in the coordinate system X, Y, Z will be

$$\begin{aligned} \omega_X &= \Omega + \dot{\Theta}\, sin\Psi \approx \Omega + \dot{\Theta}\Psi \\ \omega_Y &= \dot{\Theta}\, cos\Psi \approx \dot{\Theta} \\ \omega_Z &= \dot{\Psi} \end{aligned} \tag{2}$$

Considering the fact, that $\dot{\Theta}^2\dot{\Psi}^2 << \Omega^2$, the equation for the kinetic energy becomes

$$E_K = \frac{1}{2} J_X \Omega^2 + J_X \Omega\Psi\dot{\Theta} + \frac{1}{2}\left(J_Y \dot{\Theta}^2 + J_Z \dot{\Psi}^2\right) \tag{3}$$

The first part of equation 3 is independent of both Θ and Ψ, and thus it does not appear in Lagrange's equation. The potential energy then becomes

$$E_P = \frac{1}{2} K_\Theta \Theta^2 + \frac{1}{2} K_\Psi \Psi^2 \tag{4}$$

For a description of the structural damping we use

$$D = \frac{1}{2}\frac{K_\Theta \gamma_\Theta}{\omega}\dot{\Theta}^2 + \frac{1}{2}\frac{K_\Psi \gamma_\Psi}{\omega}\dot{\Psi}^2 \tag{5}$$

Then, we obtain from Lagrange's equations and equations 3 - 5, a system of two mutually influenced differential equations:

$$\begin{aligned} J_Y\ddot{\Theta} + \frac{K_\Theta \gamma_\Theta}{\omega}\dot{\Theta} + J_X \Omega\dot{\Psi} + K_\Theta \Theta = Q_\Theta \\ J_Z\ddot{\Psi} + \frac{K_\Psi \gamma_\Psi}{\omega}\dot{\Psi} - J_X \Omega\dot{\Theta} + K_\Psi \Psi = Q_\Psi \end{aligned} \tag{6}$$

The generalized propeller forces and moments (see figure 5) can be expressed as

$$\begin{aligned} Q_\Theta &= M_{Y,P} - aP_Z \\ Q_\Psi &= M_{Z,P} + aP_Y \end{aligned} \tag{7}$$

The index P means that the moment around the specific axis is at the plane of the propeller's rotation. Employing quasi-steady theory, the effective angles become

$$\begin{aligned} \Theta^* &= \Theta - \frac{\dot{Z}}{V_\infty} = \Theta - \frac{a\dot{\Theta}}{V_\infty} \\ \Psi^* &= \Psi - \frac{\dot{Y}}{V_\infty} = \Psi - \frac{a\dot{\Psi}}{V_\infty} \end{aligned} \tag{8}$$

Neglecting the aerodynamic inertia terms ($\dot{\Theta}^* \approx \dot{\Theta}$, $\dot{\Psi}^* \approx \dot{\Psi}$), we obtain the equations for the propeller dimensionless forces and moments as follows:

$$\begin{aligned} P_Y &= q_\infty F_p\left(c_{y\Psi}\Psi^* + c_{y\Theta}\Theta^* + c_{yq}\frac{\dot{\Theta}^* R}{V_\infty}\right) \\ P_Z &= q_\infty F_p\left(c_{z\Theta}\Theta^* + c_{z\Psi}\Psi^* + c_{zr}\frac{\dot{\Psi}^* R}{V_\infty}\right) \\ M_{Y,P} &= q_\infty F_P D_P\left(c_{m\Psi}\Psi^* + c_{mq}\frac{\dot{\Theta}^* R}{V_\infty}\right) \\ M_{Z,P} &= q_\infty F_P D_P\left(c_{n\Theta}\Theta^* + c_{nr}\frac{\dot{\Psi}^* R}{V_\infty}\right) \end{aligned} \tag{9}$$

where F_P is the propeller disc area, and D_P is the propeller diameter.

The aerodynamic derivatives are defined as follows:

$$
\begin{aligned}
&c_{y\Theta}=\frac{\partial c_y}{\partial\Theta^*} \quad c_{y\Psi}=\frac{\partial c_y}{\partial\Psi^*} \quad c_{yq}=\frac{\partial c_y}{\partial\left(\frac{\dot{\Theta}R}{V_\infty}\right)} \quad c_{yr}=\frac{\partial c_y}{\partial\left(\frac{\dot{\Psi}R}{V_\infty}\right)}\\
&c_{z\Theta}=\frac{\partial c_z}{\partial\Theta^*} \quad c_{z\Psi}=\frac{\partial c_z}{\partial\Psi^*} \quad c_{zq}=\frac{\partial c_z}{\partial\left(\frac{\dot{\Theta}R}{V_\infty}\right)} \quad c_{zr}=\frac{\partial c_z}{\partial\left(\frac{\dot{\Psi}R}{V_\infty}\right)}\\
&c_{m\Theta}=\frac{\partial c_m}{\partial\Theta^*} \quad c_{m\Psi}=\frac{\partial c_m}{\partial\Psi^*} \quad c_{mq}=\frac{\partial c_m}{\partial\left(\frac{\dot{\Theta}R}{V_\infty}\right)} \quad c_{mr}=\frac{\partial c_m}{\partial\left(\frac{\dot{\Psi}R}{V_\infty}\right)}\\
&c_{n\Theta}=\frac{\partial c_n}{\partial\Theta^*} \quad c_{n\Psi}=\frac{\partial c_n}{\partial\Psi^*} \quad c_{nq}=\frac{\partial c_n}{\partial\left(\frac{\dot{\Theta}R}{V_\infty}\right)} \quad c_{nr}=\frac{\partial c_n}{\partial\left(\frac{\dot{\Psi}R}{V_\infty}\right)}
\end{aligned}
\tag{10}
$$

These aerodynamic derivatives can be obtained analytically according to [2], [3], [4]. Due to the symmetry, the above can be expressed as follows:

$$c_{z\Psi} = c_{y\Theta}\ ;\ c_{m\Psi} = -c_{n\Theta}\ ;\ c_{mq} = c_{nr}\ ;\ c_{zr} = c_{yq}\ ;\ c_{z\Theta} = -c_{y\Psi}\ ;\ c_{n\Psi} = c_{m\Theta}\ ;\ c_{mr} = -c_{nq}\ ;\ c_{yr} = -c_{zq} \tag{11}$$

Neglecting the low-value derivatives, we can consider:

$$c_{mr} = -c_{nq} = 0\ ;\ c_{yr} = -c_{zq} = 0 \tag{12}$$

Substituting from equation 10 into the equations of motion (equation 6) considering the harmonic motion:

$$[\Theta,\Psi] = [\overline{\Theta},\overline{\Psi}]e^{j\omega t} \tag{13}$$

We obtain the final whirl flutter matrix equation:

$$\left(-\omega^2[M]+j\omega\left([D]+[G]+q_\infty F_P\frac{D_P^2}{V_\infty}[D^A]\right)+\left([K]+q_\infty F_P D_P[K^A]\right)\right)\left|\begin{matrix}\overline{\Theta}\\ \overline{\Psi}\end{matrix}\right| = \{0\} \tag{14}$$

The solution can be found by treating the problem as an eigenvalue problem. The limit (flutter) state is attained when there is a specific combination of the parameters V_∞ and Ω, that cause the angular velocity ω to become a real number. The whirl flutter characteristics are explained in figure 6, which describes the influence of the propeller's advance ratio ($V_\infty/(\Omega R)$) on the stability of an undamped gyroscopic system. Increasing the propeller's advance ratio causes an increase in the required stiffnesses, K_Θ, K_Ψ.

In general, the whirl flutter appears at the gyroscopic rotational vibrations, and the flutter frequency is the same as the frequency of the backward gyroscopic mode. The critical state can be reached due to increasing either the air velocity or the propeller revolutions. Structural damping is a significant stabilization factor. In contrast, the propeller thrust influence is barely noticeable. The most critical state is $K_\Theta = K_\Psi$, which means $\omega_\Theta = \omega_\Psi$, for which the interaction of the two independent motions is maximal. A special case of equation 14 for $\omega = 0$ is the gyroscopic static divergence, which is obtained when the determinant of the whirl flutter matrix becomes zero. In the case of divergence, the motion loses its oscillatory character, and the unstable motion becomes unidirectional. The divergence can appear when either the pitch or yaw stiffness decreases to be under a specific threshold; however, it is worthwhile to comment, that when the stiffness values of $K_\Theta \approx K_\Psi$ approach the zero, the divergence does not appear.

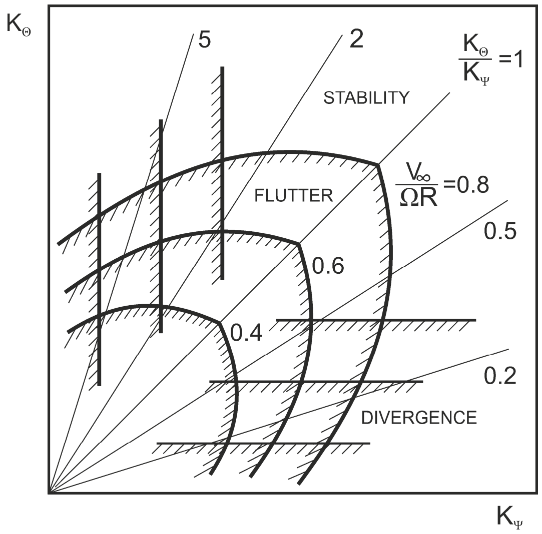

Figure 6: Influence of the propeller's advance ratio on the stability of the undamped gyroscopic system

3. Solution and Reference Model

The commonly used solution for whirl flutter analysis is the usage of standard FE code (NASTRAN), which is supplemented by in-house code for the solution of the propeller aerodynamic and gyroscopic terms (*propfm*). The NASTRAN program system is used worldwide, especially in the aerospace and automotive industries. NASTRAN is a standard computational tool for various types of aeroelastic analyses; therefore, it is easy to use the same FE model and incorporate the whirl flutter analysis into the whole aeroelastic certification procedure. The whirl flutter calculation is based on flutter solver nr.145 (standard approach) or optionally on optimization solver nr.200 (optimization-based approach). The whirl flutter solution is supported by the DMAP program (*propa.alt* or *propa_200.alt*). A propeller's aerodynamic forces as well as the gyroscopic terms are calculated by means of the mentioned external program (*propfm*). These terms are formally included into the stiffness and damping matrices respectively, i.e., the output data are included into the NASTRAN input file. Both of these analytical approaches as well as the other aspects of the NASTRAN-based solution of the whirl flutter and the description of the *propfm* code can be found in [11].

As an option, there is a possibility of including the interference effects between the propeller, nacelle and wing by means of reduced frequency dependent downwash and sidewash effects. In this case, two or more NASTRAN runs are employed. The first set of runs generates downwash and sidewash angles, and then, a calculation is terminated. This calculation is performed for each rotor separately, i.e., in two NASTRAN runs for a twin engine aircraft. The downwash data are processed by the *propfm* preprocessor and included again in the NASTRAN file. The last NASTRAN run then makes the final stability solution.

Considering the standard twin wing-mounted engine aircraft configuration, the analysis can be performed by means of a half-span model with the symmetric and antisymmetric boundary condition or by a full-span model. Obviously, the usage of the half-span model is limited, as described later. To be able to handle multiple rotors, an improved version of the *propfm* code (version 3) was created. The improved program handles multiple rotors independently. The engine inertia, propeller geometry and aerodynamic data are expected to be the same for all of the rotors. In contrast, a propeller's revolutions with respect to a rotational speed and direction can be set arbitrarily, and the propeller blade integrals, the lag effects (provided are included) and, finally, the aerodynamic derivatives and the stiffness and damping term calculations are performed for each rotor separately.

The workflow of the complete procedure of the NASTRAN-based whirl flutter analysis for a twin-engine aircraft configuration is shown in figure 7. Note that the workflow also includes further blocks for the correction of the aerodynamic model and for post-processing of the output data.

A reference model that was used for the presented calculations was derived from the model of an EV-55M turboprop utility aircraft (figure 8), which holds 9 - 13 passengers. This aircraft has a total length of 14.35 m, a wingspan of 16.10 m and a maximal take-of weight of 4600 kg. It is powered by two PT6A-21 turboprop engines with AV-844 four-blade constant speed propellers.

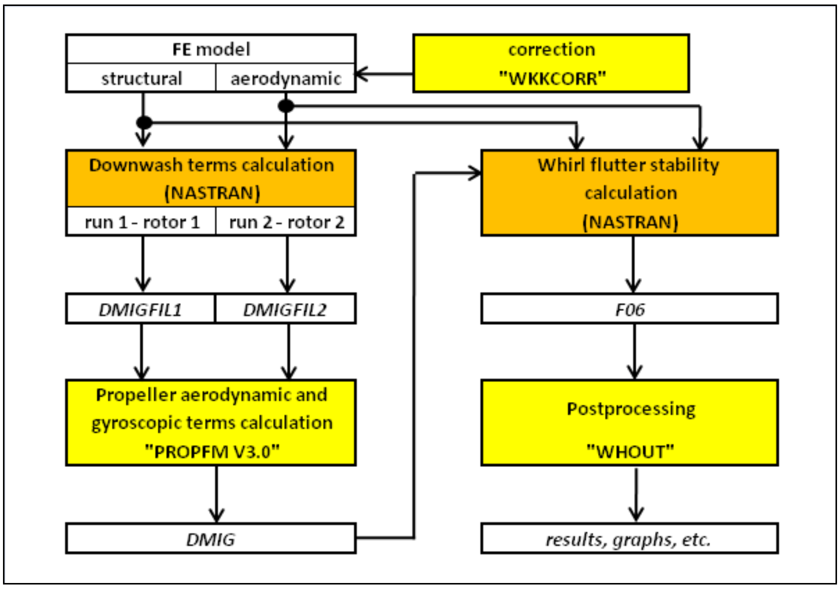

Figure 7: Whirl flutter analysis using a NASTRAN - workflow

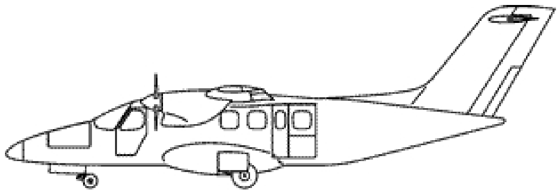

Figure 8: EV-55M aircraft

We used a dynamic stick model of the reference aircraft. The inertia characteristics were modelled using concentrated mass elements with appropriate moments of inertia. For the purpose of the presented analyses, the stiffness characteristics, which were modelled using beam elements, were replaced by rigid connections. The control surface and tab drives were blocked. Only the flexible attachment of the engines by means of spring elements remained. In fact, the model has four degrees-of-freedom, which are both the symmetric and antisymmetric engine pitch and yaw vibrations. This simplification helped us to assess the influences of the specific parameters. An aerodynamic model included Doublet-Lattice Panels (wing, tail) combined with Slender and Interference Bodies (fuselage, nacelle). The aerodynamic model included also correction factors for the propeller slipstream applied to the appropriate aerodynamic elements of the wing and nacelles. Furthermore, there is also a correction in the aerodynamic forces and moments at the nose part of the control surfaces. Basically, the full-span model shown in figure 9 was used for the analyses. Optionally, the half-span model with either symmetric or antisymmetric boundary conditions and a correction of the aerodynamic model for the plane of symmetry were used for comparative analyses.

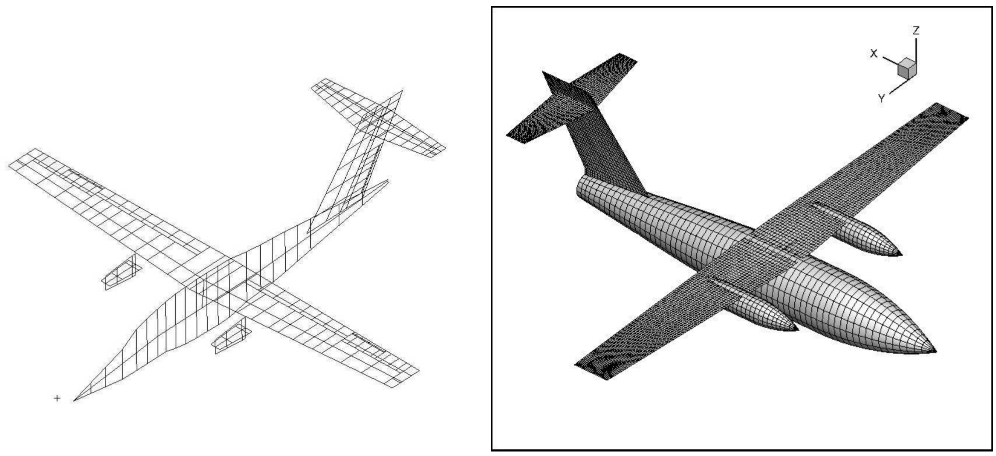

a) b)

Figure 9: Reference structure full-span model (a) structural, and (b) aerodynamic

The whirl flutter-related data included the inertia, geometry and aerodynamics of the power plant system, i.e., the PT6A-21 engine and Avia AV-844 propeller. Both the identical and inverse revolutions of both propellers were considered. The former case was considered to be the clockwise revolutions of both propellers (CW/CW), while the latter case was considered to be the clockwise revolutions of the left propeller and the counter-clockwise revolutions of the right propeller (CW/CCW). Note that both cases do not have a physical interpretation because the EV-55 aircraft propellers both rotate in a counter-clockwise direction. Thus, both cases represent artificial states. The propeller nominal revolutions were set at $\Omega = 2200$ rpm. Additionally, the data for the non-symmetric cases were prepared for both of the above mentioned options of the propeller rotations. The non-symmetric cases included a single propeller feathering (only the left rotor was included), a single propeller overspeed (an increase in the revolutions of the right rotor by 15%), and finally, the reduced revolutions of a single (right) propeller (reduced by 15%). The analyses did not include the downwash effect.

Analyses were performed using an optimization-based approach [11]. The results of optimization-based analyses are the critical values of the structural parameters, for which the critical flutter speed is equal to the selected value. These analyses are used to draw the stability margins, typically with respect to the engine attachment stiffness or to the engine vibration frequencies. Analyses were performed for $V_{FL} = 1.2V_D$, which is the certification velocity according to the regulation standard FAR/CS 23 [5], [6], [7]. The value of $1.2V_D$ at the analysed altitude of H = 3100 m is 176 m.s^{-1}. Analyses were performed as non-matched analyses, i.e., using a single (reference) Mach number $M = M_D = 0.446$. The PK method of the flutter stability solution was employed. The selected mass configuration of the aircraft included 50% of the fuel, two passengers in the 3rd row and statically balanced control surfaces.

4. Analyses and Results

The reference model represents the rigid aircraft structure with flexibly attached engines. The model includes four degrees-of-freedom: antisymmetric pitch vibrations, symmetric pitch vibrations, symmetric yaw vibrations and antisymmetric yaw vibrations, as depicted in figure 10.

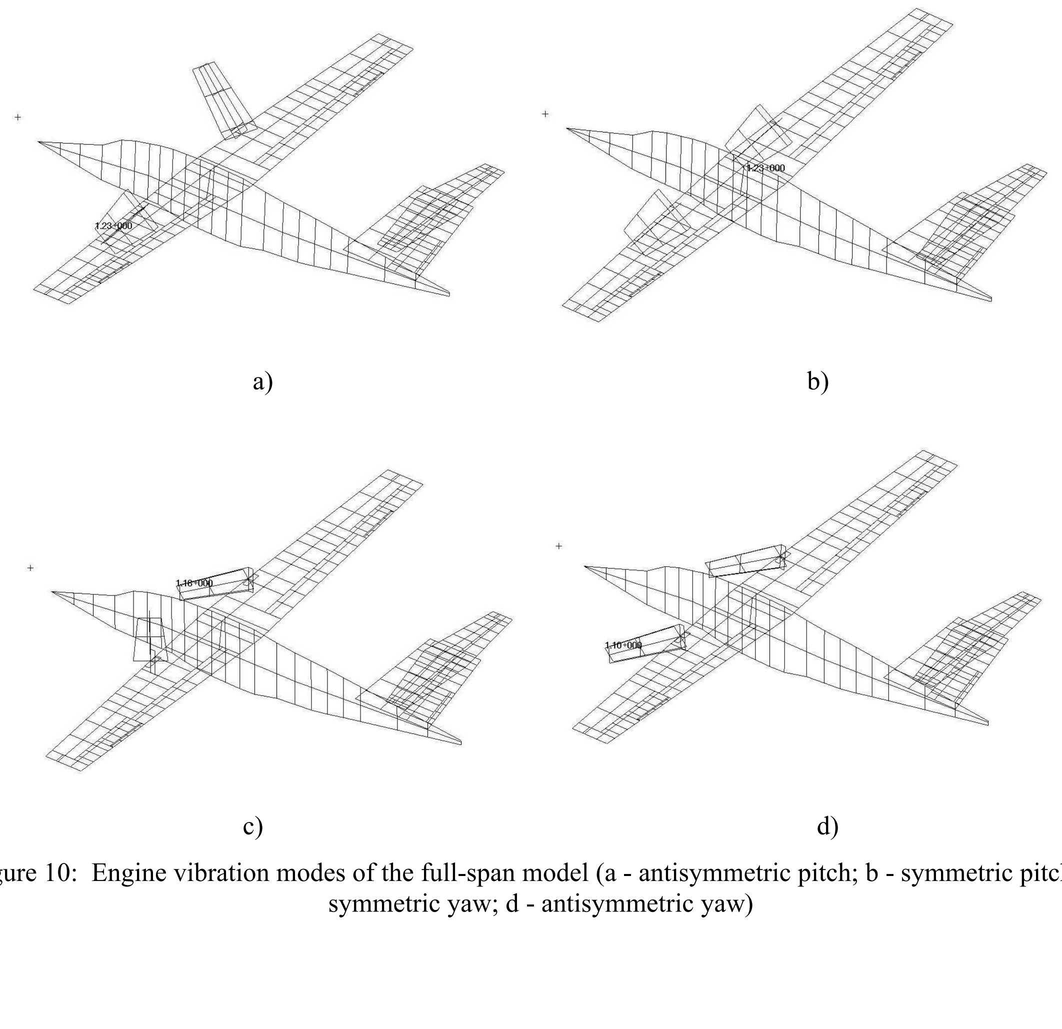

Figure 10: Engine vibration modes of the full-span model (a - antisymmetric pitch; b - symmetric pitch; c - symmetric yaw; d - antisymmetric yaw)

First, analyses of the symmetric revolutions of the two propellers were performed. These analyses were aimed at demonstrating the influence of the relationship of the propeller revolutions, i.e., CW/CW and CW/CCW. Analyses using full-span models were supplemented by the analyses that used the half-span model, with the appropriate boundary conditions.

Considering the identical rotations (CW/CW), two mechanisms for the whirl flutter appear: 1) a combination of symmetric pitch and antisymmetric yaw modes (SP/AY) and 2) a combination of antisymmetric pitch and symmetric yaw modes (AP/SY). The stability margins were calculated with respect to both of the mechanisms of whirl flutter. As is apparent from the figures, the required engine pitch and yaw stiffness (or required engine pitch and yaw frequency) is higher for the former mechanism of whirl flutter.

Considering the inverse rotations (CW/CCW), the character of the whirl flutter is different. The instability is caused by the combination of symmetric pitch and symmetric yaw modes (SP/SY) for the higher yaw-to-pitch stiffness ratios or is caused by the combination of antisymmetric pitch and antisymmetric yaw modes (AP/AY) for the low yaw-to-pitch stiffness ratios. These types of instability represent the lower and upper arm of the stability margin. Compared to the CW/CW case, the required engine pitch and yaw stiffness (or required engine pitch and yaw frequency) is considerably higher.

Considering the half-span model with the symmetric boundary condition, the resulting stability margin is close to the stability margin of a combination of symmetric pitch and antisymmetric yaw modes for the CW/CW rotations of the full-span model. Considering the half-span model with the antisymmetric boundary condition, the resulting stability margin is close to that of a combination of antisymmetric pitch and symmetric yaw modes for the CW/CW rotations of the full-span model. These facts justify the usage of the half-span model for the whirl flutter calculations; however, the applicability of the half-span model is obviously limited to identical propeller revolutions (CW/CW). Note that the case in which there are identical revolutions is the most common case for small aircraft.

Figures 11 and 12 show the mentioned stability margins. Figure 11 represents the required engine attachment pitch and yaw stiffness, while figure 12 represents the required pitch and yaw engine vibration mode frequency.

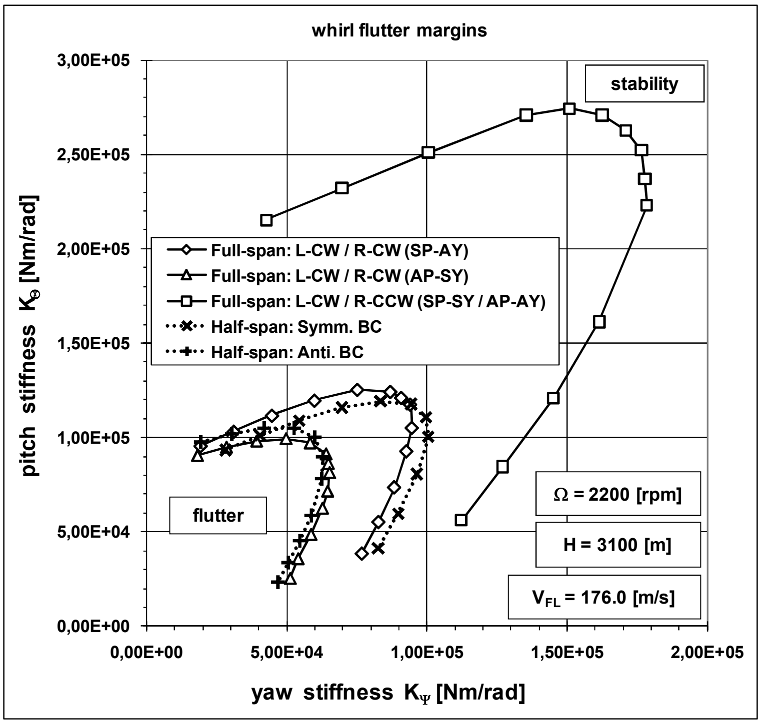

Figure 11: Whirl flutter stability margins - required pitch and yaw stiffness: Comparison of the flutter mechanisms (full-span model (CW/CW and CW/CCW), half-span model (symmetric (symm.) and antisymmetric (anti.) boundary condition (BC))

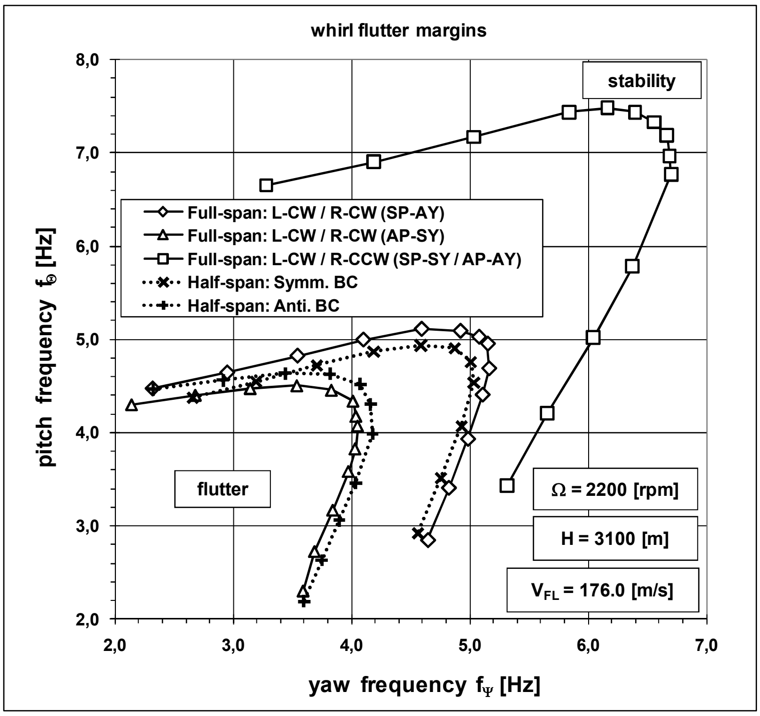

Figure 12: Whirl flutter stability margins - required pitch and yaw frequency: Comparison of the flutter mechanisms (full-span model (CW/CW and CW/CCW), half-span model (symmetric (symm.) and antisymmetric (anti.) boundary condition (BC))

The next calculations were aimed at demonstrating the non-symmetric cases with respect to the propeller revolutions, and the following cases are included:

1) Case of a feathered single propeller: Left propeller: Ω_L = 2200 rpm; Right propeller: Ω_R = 0 rpm

2) Case of reduced revolutions of a single propeller, reduced by 15%: Left propeller: Ω_L = 2200 rpm; Right propeller: Ω_R = 1870 rpm

3) Case of a single propeller having overspeed by 15%: Left propeller: Ω_L = 2200 rpm; Right propeller: Ω_R = 2530 rpm

The following diagrams show comparisons of the stability margins in reference the baseline case in which there are symmetric revolutions. Figures 13 and 14 show the case of the CW/CW rotations. These figures include the baseline cases of rpm 2200/2200 considering both SP/AY and AP/SY for the whirl flutter mechanisms. Non-symmetric revolutions are represented by rpm 2200/1870 and rpm 2200/2530. For these non-symmetric cases, only the margin for the more critical SP/AY whirl flutter mechanism is included. Finally, the figures include the case of rpm 2200/0, which represents the state of a single propeller that undergoes feathering. However, for this case, the only flutter mechanism that appears is AP/SY.

The most critical cases are those of rpm 2200/2200 SP/AY and rpm 2200/2530 SP/AY. However, considering the fact that the yaw frequency is usually higher than the pitch frequency, the lower arm of the margin curve has a physical interpretation, and thus, the case of rpm 2200/2530 SP/AY should be considered to be the most critical case with a physical interpretation. Considering the AP/SY flutter mechanism, the case of rpm 2200/0 is more unstable compared to the symmetric case.

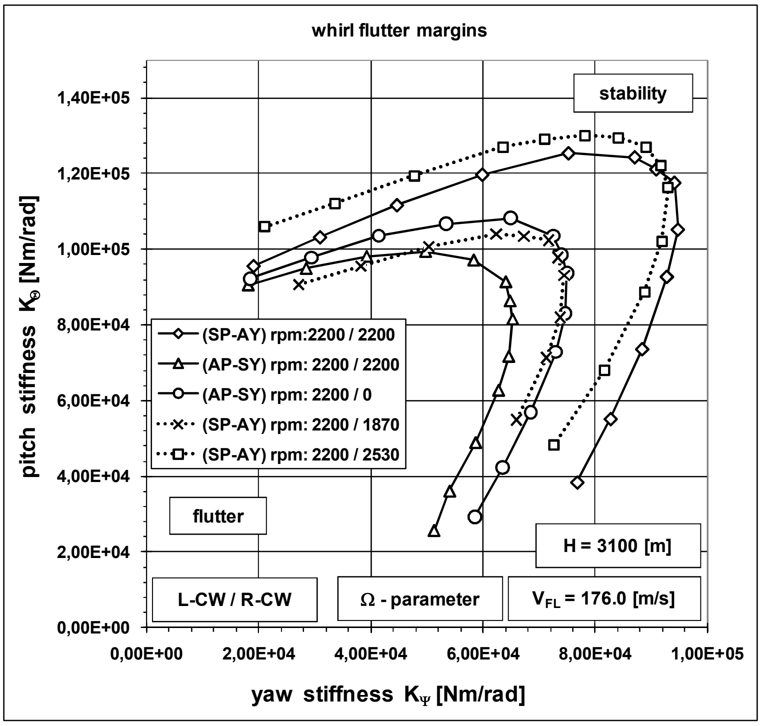

Figure 13: Whirl flutter stability margins - required pitch and yaw stiffness, full-span model, (CW/CW), parameter: propeller revolutions (including non-symmetric cases)

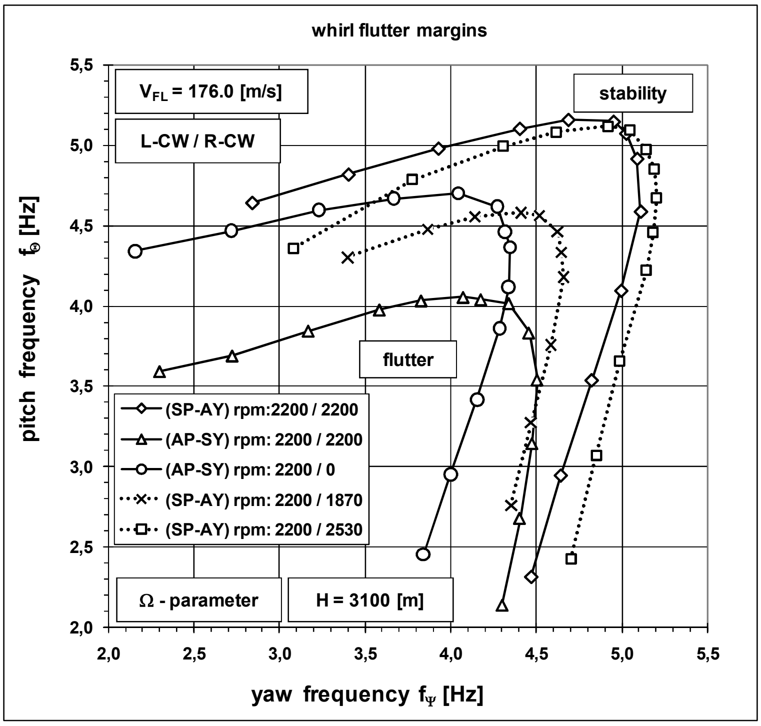

Figure 14: Whirl flutter stability margins - required pitch and yaw frequency, full-span model, (CW/CW), parameter: propeller revolutions (including non-symmetric cases)

Figures 15 and 16 show the case of the CW/CCW rotations. These figures include the baseline case of rpm 2200/2200 and the non-symmetric cases that are represented by rpm 2200/1870 and rpm 2200/2530. The most critical case is the case of the propeller overspeed (rpm 2200/2530), regardless of the yaw-to-pitch frequency ratio.

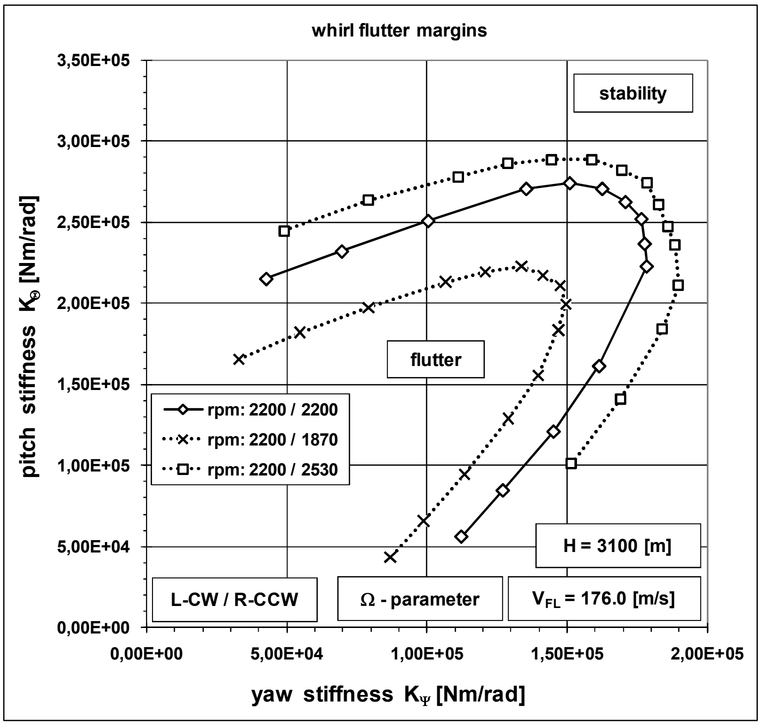

Figure 15: Whirl flutter stability margins - required pitch and yaw stiffness, full-span model, (CW/CCW), parameter: propeller revolutions (including non-symmetric cases)

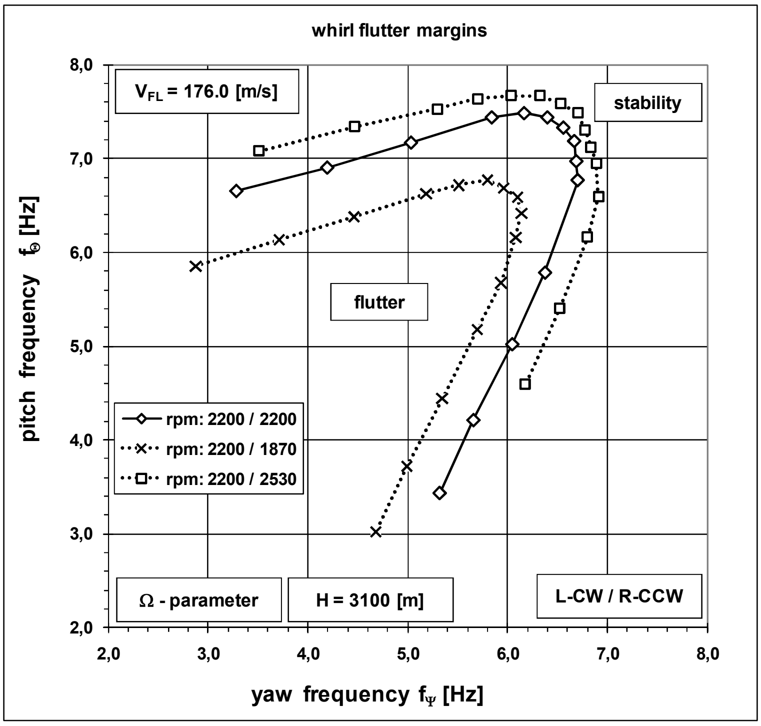

Figure 16: Whirl flutter stability margins - required pitch and yaw frequency, full-span model, (CW/CCW), parameter: propeller revolutions (including non-symmetric cases)

5. Conclusions and Outlook

This paper presents an assessment of the parameters of a propeller rotation, i.e., the direction of rotation and the revolutions with respect to the characteristics in whirl flutter of a twin wing-mounted engine turboprop aircraft. The analyses include both identical (CW/CW) and inverse (CW/CCW) relations of propeller revolutions as well as the non-symmetric cases (a single propeller feathering, a single propeller overspeed, rpm reduction of a single propeller). A reference structure with four degrees-of-freedom derived from a model of the EV-55 utility turboprop aircraft was employed for the evaluation. The typical mechanisms of whirl flutter for both cases are shown, and the most critical flutter types are evaluated. For this purpose, an optimization-based approach by means of NASTRAN solver 200 was used. This approach allowed us to evaluate flutter margins with respect to structural parameters, such as the engine mount stiffness or the engine pitch and yaw frequencies. The analyses that use the full-span model are supplemented by analyses that use the half-span model, and the applicability of the half-span model is defined and justified. Usage of the half-span model increases the effectiveness of the work; however, the applicability of the half-span model is limited only to the case of identical directions of propeller rotation, which is, nevertheless the most common case. Other cases, typically the non-symmetric cases, can be solved using a full-span model only.

Depending on the relationships among the propeller directions of rotation, different flutter mechanisms were found. For the case of identical directions (CW/CW), flutter is formed by coupling the symmetric pitch and antisymmetric yaw or by coupling the antisymmetric pitch and symmetric yaw. The former flutter mechanism can be simulated also by the half-span model with a symmetric boundary condition, the latter flutter mechanism can be simulated by the half-span model with an antisymmetric boundary condition. The former case is less stable, i.e., it requires a higher engine pitch and yaw stiffness (or frequency). Considering the pitch frequency to be lower compared to the yaw frequency, which is the most common case in the practice, the most critical case is a single propeller overspeed; however, this case is comparable to the case of symmetric revolutions. For the case of inverse directions (CW/CCW), flutter is formed by the coupling the symmetric pitch and symmetric yaw or by the coupling the antisymmetric pitch and antisymmetric yaw. Considering the pitch frequency to be lower compared to the yaw frequency, the former is the case with the physical interpretation. The most critical case is a single propeller overspeed.

The comparison of the stability margins of both the CW/CW and CW/CCW cases shows, that the latter is evidently less stable compared to the former, regardless of the propeller revolutions.

The presented work does not include an evaluation of the influence of the engine vibration node points. There were coincident node points in both the symmetric and antisymmetric vibrations; however, in practice, the nodal points of the antisymmetric vibration modes are usually forward compared to the symmetric modes. Further investigation will include the evaluation of the engine stiffness asymmetry, e.g., due to a failure of a load-bearing element in a single engine mount. Additionally, the assessment of the downwash effect for both the CW/CW and CW/CCW cases of the propeller directions of rotation will be a subject of future work.

References

[1] Taylor, E. S., Browne, K. A. 1938. Vibration Isolation of Aircraft Power Plants, *Journal of Aerospace Sciences*, Vol.6, no.2, pp. 43-49.

[2] Ribner, H. S. 1943. Formulas for Propellers in Yaw and Charts of the Side – Force Derivatives, NACA Report 819.

[3] Ribner, H.S. 1945. Propellers in Yaw, NACA Report 820.

[4] Houbolt, J.C., Reed, W.H. 1962. Propeller – Nacelle Whirl Flutter, *Journal of Aerospace Sciences*, Vol.29, No.3, pp.333-346.

[5] European Aviation Safety Agency. 2012. CS-23, Amdt.3 - Certification Specifications for Normal, Utility, Aerobatic, and Commuter Category Aeroplanes.

[6] US. Department of Transportation, Federal Aviation Administration. 2012. FAR-23, Amdt.62 - Federal Aviation Regulations, Part 23: Airworthiness Standards: Normal, Utility, Acrobatic and Commuter Category Airplanes.

[7] US. Department of Transportation, Federal Aviation Administration. 2004. AC-23.629-1B, Means of Compliance with Title 14 CFR, Part 23 §23.629, Flutter, Advisory Circular.

[8] European Aviation Safety Agency. 2012. CS-25, Amdt.12 - Certification Specifications and Acceptable Means of Compliance for Large Aeroplanes CS-25.

[9] US. Department of Transportation, Federal Aviation Administration. 2012. FAR-25, Amdt.135 - Federal Aviation Regulations, Part 25: Airworthiness Standards: Transport Category Airplanes, FAR-25.

[10] Reed, W. H. 1967. Review of Propeller - Rotor Whirl Flutter, NASA Technical Report, NASA TR R-264.

[11] Cecrdle, J. 2015. Whirl Flutter of Turboprop Aircraft Structures, Elsevier Science, Ltd., ISBN 978-1-78242-185-6